Atomic-Scale Simulations of Meteor Ablation

Gabrielle Guttormsen[1], Alex Fletcher[2], and Meers M. Oppenheim[1]

[1]Boston University
[2]Unknown

November 24, 2022

Abstract

Meteoroids smaller than a microgram constantly bombard the Earth, depositing in the mesosphere and lower thermosphere. Meteoroid ablation, the explosive evaporation of meteoroids due to erosive impacts of atmospheric particles, consists of sputtering and sublimation. This paper presents the first atomic scale modeling of sputtering, the initial stage of ablation where hypersonic collisions between the meteoroid and atmospheric particles cause the direct ejection of atoms from the meteoroid surface. Because meteoroids gain thermal energy from these particle impacts, these interactions are important for sublimation as well. In this study, a molecular dynamics simulator calculates the energy distribution of the sputtered particles as a function of the species, velocity, and angle of the incoming atmospheric particles. The sputtering yield generally agrees with semi-empirical equations at normal incidence but disagrees with the generally accepted angular dependence. Λ, the fraction of energy from a single atmospheric particle impact incorporated into the meteoroid, was found to be less than 1 and dependent on the velocity, angle, atmospheric species, and meteoroid material. Applying this new Λ to an ablation model results in a slower meteoroid temperature increase and mass loss rate as a function of altitude. This alteration results in changes in the expected electron line densities and visual magnitudes of meteoroids. Notably, this analysis leads to the prediction that meteoroids will generally ablate 1 - 4 km lower than previously predicted. This affects analysis of radar and visual measurements, as well as determination of meteoroid mass.

Supporting Information for "Atomic-Scale Simulations of Meteor Ablation"

Gabrielle Guttormsen[1], Alex C. Fletcher[2], and Meers M. Oppenheim[1]

[1]Center for Space Physics, Boston University, Boston, MA, USA
[2]Naval Research Laboratory, Washington D.C., USA

Additional Supporting Information (Files uploaded separately)

1. Caption for Movie S1

Movie S1.

This movie shows a LAMMPS simulation of an normally incident argon atom impact on a quartz (SiO_2) target. The color scale shows the kinetic energy of the atoms, with black to red indicating lower energies, and orange to yellow and white indicating higher energies. The white atoms leaving the surface are the sputtered atoms, and disappear from the simulation after crossing the upper boundary. The simulation block is approximately 145 Åin the x and y direction, and 70 Åin the z direction. The simulation view is in the x-z plane.

Corresponding author: Gabrielle Guttormsen, gabigutt@bu.edu

Atomic-Scale Simulations of Meteor Ablation

Gabrielle Guttormsen[1], Alex C. Fletcher[2], and Meers M. Oppenheim[1]

[1]Center for Space Physics, Boston University, Boston, MA, USA
[2]Naval Research Laboratory, Washington D.C., USA

Key Points:

- Single particle impacts on meteoroid surfaces were simulated in 3D using molecular dynamics
- Sputtering yields for different meteoroid materials are compared to theory
- Atmospheric particles energy transfer is less than previously assumed affecting ablation models

Corresponding author: Gabrielle Guttormsen, `gabigutt@bu.edu`

Abstract

Meteoroids smaller than a microgram constantly bombard the Earth, depositing material in the mesosphere and lower thermosphere. Meteoroid ablation, the explosive evaporation of meteoroids due to erosive impacts of atmospheric particles, consists of sputtering and sublimation. This paper presents the first atomic scale modeling of sputtering, the initial stage of ablation where hypersonic collisions between the meteoroid and atmospheric particles cause the direct ejection of atoms from the meteoroid surface. Because meteoroids gain thermal energy from these particle impacts, these interactions are important for sublimation as well. In this study, a molecular dynamics simulator calculates the energy distribution of the sputtered particles as a function of the species, velocity, and angle of the incoming atmospheric particles. The sputtering yield generally agrees with semi-empirical equations at normal incidence but disagrees with the generally accepted angular dependence. Λ, the fraction of energy from a single atmospheric particle impact incorporated into the meteoroid, was found to be less than 1 and dependent on the velocity, angle, atmospheric species, and meteoroid material. Applying this new Λ to an ablation model results in a slower meteoroid temperature increase and mass loss rate as a function of altitude. This alteration results in changes in the expected electron line densities and visual magnitudes of meteoroids. Notably, this analysis leads to the prediction that meteoroids will generally ablate 1 - 4 km lower than previously predicted. This affects analysis of radar and visual measurements, as well as determination of meteoroid mass.

1 Introduction

Billions of small meteoroids vaporize in Earth's atmosphere each day. The majority of these meteoroids weigh less than a milligram and have velocities ranging from 11 km/s to 72 km/s (Love & Brownlee, 1991). Meteoroids begin to lose mass (ablate) once they collide with atmospheric particles. The neutral atmosphere becomes exponentially denser with decreasing altitude, which exponentially increases the collision rate. The liberated meteoroid atoms collide with atmospheric particles, forming plasma via collisional ionization. Radars often observe the liberated electron.

There are two mechanisms for meteoroid ablation in the atmosphere: sputtering and sublimation. Sputtering is the direct ejection of a small number of atoms from the meteoroid due to impacts by atmospheric particles. It is the dominant ablation process for very small and very fast meteoroids (Rogers et al., 2005). Sublimation occurs when the meteoroid reaches a sufficiently high temperature ($\gtrsim$ 2200 K) and dominates the mass loss (Ceplecha et al., 1998). However, the single particle impacts influence the heating rate of the meteoroid, which determines when the sublimation rate as well. Fig. 1 depicts an example of this process.

Each impact by an atmospheric particle on the meteoroid surface has a chance to dislodge (sputter) a small number of meteoroid atoms (on average 0, 1, or 2 atoms per impact, depending on meteoroid velocity). These sputtered particles carry away energy from the meteoroid. The incident atmospheric particle therefore transfers some, but generally not all, of its kinetic energy to the meteoroid in the form of increased thermal energy. The fraction of kinetic energy that is converted to thermal energy, averaged over many impacts, is the energy transfer coefficient, Λ. This coefficient is a function of meteoroid velocity, shape, and the material makeup of the meteoroid and atmosphere (which changes with altitude). Most ablation models assume $\Lambda = 1$ (e.g. Rogers et al., 2005; Vondrak et al., 2008; Briani et al., 2013), and this assumption will overestimate the heating rate and therefore the mass loss rate from sublimation.

In this paper, we use atomic scale molecular dynamics (MD) simulations to model impacts of atmospheric particles on meteoroid surfaces. We consider a range of mete-

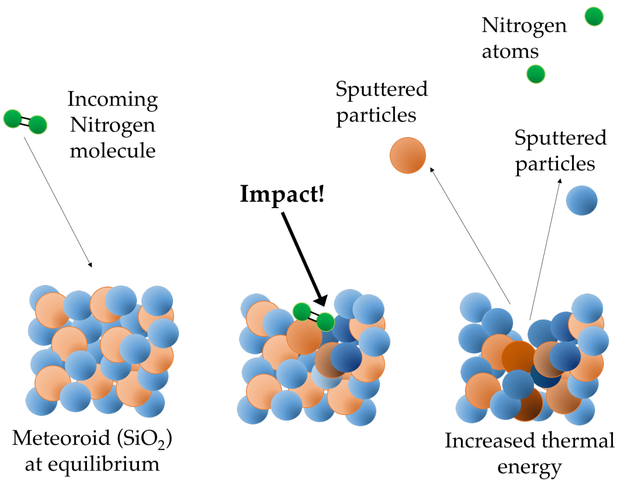

Figure 1. This image shows a nitrogen molecule from the atmosphere striking a stony meteoroid. Two atoms from the meteoroid are sputtered and the thermal energy of the meteoroid body increases.

oroid velocities, impact angles, meteoroid materials, and incident atmospheric particles. We simulate each type of impact hundreds of times in order to determine average sputtering yields (which is the number of atoms leaving the surface meteoroid due to a single impact), the energy distribution of sputtered particles, and the energy transfer coefficient (Λ). The microscopic simulation data provides macroscopic coefficients necessary for meteoroid ablation models. We then show how a reduced energy transfer coefficient ($\Lambda < 1$) affects the mass loss rate, as well as derived radar/optical observables (Campbell-Brown & Koschny, 2004; Szasz et al., 2008; Vida et al., 2018; Dimant & Oppenheim, 2017a, 2017b).

Models assume Λ =1.0, so energy from atmospheric impacting atmospheric particles is completely incorporated into the meteoroid (Lebedinets & Shushkova, 1970; Ceplecha et al., 1998; Rogers et al., 2005; Hill et al., 2005). Others assume that half the initial energy is transferred the meteoroid (Campbell-Brown & Koschny, 2004; Vida et al., 2018). Models that fit to data use a range of values from 0.2-1.0 (Szasz et al., 2008; Thomas, 2017). Briani et al. (2013) calculate the Λ as an output of their numerical model (0.9 for low velocities) and Popova, Strelkov, and Sidneva (2007) calculates Λ with energy ratios from Monte-Carlo simulations, finding Λ between 0.75 and 1.0. Experimentally, DeLuca and Sternovsky (2019) used a measured drag coefficient to constrain the energy transfer coefficient to Λ =0.58$\pm$0.37 for a low velocity aluminum target in air. MD simulations with physical interatomic potentials can provide an estimate for the energy transfer coefficient as well, and this is the subject of the paper.

Researchers have used analytic theory, experiments, and simulations to study sputtering. A combination of analytic theory with some experimentally-determined coefficients yields a semi-analytic model for sputtering yield (e.g. Tielens et al., 1994). Experimentalists determine sputtering yield by measuring crater depth (Laegreid & Wehner, 1961; Cheney et al., 1963; Krebs, 1977; Tsunoyama et al., 1976) or by using quartz crystal microbalance to detect changes in resonant frequencies that relate to the mass loss (Varga et al., 1997; Bouneau et al., 2002; Zoerb et al., 2005). Urbassek (1997) and Behrisch and Eckstein (2007) review the use of MD simulations to study sputtering. Most prior sputtering simulation work focuses on the detailed dynamics of the atoms in the target material. The novel aspects of this paper are the use of MD simulations to 1) determine the energy transfer coefficient, and 2) to apply the results to meteoroid ablation.

This paper is split into two parts. The first delves into microscopic simulations and the second applies the results from atomic-scale simulations to macroscopic meteor ablation models. The microscopic simulations use molecular dynamics (MD) simulations to model atmospheric impacts on the surface of meteoroids and extract the sputtering yield, energies of sputtered atoms, and energy transfer efficiency. The macroscopic meteor ablation modeling uses parameters determined from the microscopic simulations to quantify changes in meteoroid temperature, mass loss, and derived parameters relevant for radar and optical observations.

2 Simulations of Meteoroid-Atmosphere Interactions

Molecular dynamics (MD) is a useful tool for simulating the interaction of incident atmospheric particles with a meteoroid surface. MD is extremely small scale since every atom is simulated directly. Interatomic potentials provide forces for moving the atoms at each time step. We use the Large-scale Atomic/Molecular Massively Parallel Simulator (LAMMPS) (Sandia National Labs & Temple University, 2013; S. Plimpton, 1995; S. J. Plimpton & Thompson, 2012).

From the simulations, we can determine the sputtering yield (which is how many meteoroid particles are ejected per impacting particle), the energy distribution of sputtered particles, and the energy transfer coefficient (Λ, which is the fraction of kinetic energy that impacting particles deposit into the meteoroid as thermal energy). The energy transfer coefficient affects the heating rate of the meteoroid, and thus the temperature, mass loss (during both sputtering and sublimation), and ultimately the radar and optical observables of meteors.

2.1 Simulation Setup

Simulation of a the single impact of an atmospheric molecule requires two steps: 1) creating a meteoroid target in equilibrium, and 2) bombarding that target with atmospheric particles. To create a meteoroid target in equilibrium, a 3D periodic box is constructed with atoms in an appropriate crystal structure at zero Kelvin. The simulation is run with an isenthalpic integrator ("NPH" in LAMMPS) with a Langevin thermostat to gradually heat the target to 250 K. The boundaries are allowed to expand and contract as necessary. After the simulation reaches thermal equilibrium at 250 K for the periodic system, one boundary is changed to vacuum and the integration is changed to be energy conserving ("NVE" in LAMMPS) in order to form the surface that the atmospheric particle will hit, and run until the simulation reaches equilibrium again.

The equilibrium meteoroid target is used in a variety of impact simulations with different atmospheric particles hitting different locations at different angles. Because sputtering is a stochastic process, a large number of impact simulations provides statistics and allows us to determine the sputtering yield and energy transfer coefficient on average.

These simulations used two interatomic potentials to model the atomic forces. The target lattice atoms/molecules (Fe, SiO_2) respond to the Tersoff potential (Tersoff, 1988), a many-body potential suited to empirical simulations of solid, bonded materials (Müller et al., 2007; Munetoh et al., 2007). The Embedded Atom Method (EAM) potential is often used for metallic alloys like meteoroid iron. However, EAM has problems properly describing surfaces (Zhou & Huang, 2013), and microscopic surface effects dominate the sputtering process. The Tersoff potential is mainly used for covalent bonds and is an appropriate potential for the quartz lattice. The impacting particles (N_2, O_2, Ar) and the target lattice interact via the Lennard-Jones potential, due to its simplicity (Behrisch & Eckstein, 2007; Elliott, 2018). Lorentz-Berthelot combining rules determine the mixed parameters for unlike atoms (Lorentz, 1881; Berthelot, 1898).

2.2 Sputtering Yield at Normal Incidence

We first examine the sputtering yield, which is the number of sputtered particles per impacting particle, for impacts at normal incidence. Impact simulations consisted of 256 runs for each velocity and combination of incident atmospheric particle and meteoroid material. The impacting particles are nitrogen (N_2), oxygen (O_2), and Argon (Ar). N_2 and O_2 are the most common molecules in the region where meteoroids ablate. Argon is a trace particle in the atmosphere, but it has a large sputtering yield, is easier to model than molecules, and has been used for some ground-based experiments. Therefore, it is useful for examining the validity of the simulation results, and is also included. Each impact simulation begins with the identical iron or quartz equilibrium target.

A single particle is deposited above the target at a random location at one of five velocities: 23.2, 35.4, 47.6, 59.8, or 72.0 km/s. Velocities less than 22 km/s are not useful to simulate for their sputtering yield, as it is close to null. For the thermal energy transfer discussed in Section 2.5, 11 km/s impacts help determine the energy transfer coefficient, but those simulations are not included in this section.

The simulations run for 0.25 to 4 ps with a variable time-step. This duration is long enough to ensure that atoms ejected from the meteoroid surface are recorded (Behrisch & Eckstein, 2007). Fig. 2 shows one instance of an impact simulation, and animated in supporting information. The kinetic energy of the atoms near the impact site have increased - i.e. the thermal energy of the meteoroid has increased. While the increased energy in the meteoroid is localized on these extremely short time scales, Vondrak et al. (2008) argued that over the ablation time scale, meteoroids may be considered isothermal. There are a handful of atoms that have escaped the surface and will leave the domain at the top of the z-axis.

A widely used semi-analytic equation for sputtering yield at normal incidence is (Tielens et al., 1994)

$$Y(E_0, \theta = 0) = \frac{3.56}{U_0(eV)} \frac{M_1}{M_1 + M_2} \frac{Z_1 Z_2}{\sqrt{Z_1^{\frac{2}{3}} + Z_2^{\frac{2}{3}}}} s_n(\gamma) \alpha \frac{R_p}{R} \left[1 - \left(\frac{E_{th}}{E_0}\right)^{2/3}\right] \left(1 - \frac{E_{th}}{E_0}\right)^2, \quad (1)$$

where Y is the yield, U_0 is the sublimation energy in eV, and Z_1, Z_2, M_1 and M_2 are the atomic numbers and atomic masses of the atmospheric (1) and meteoroid (2) particles, respectively. E_0 is the kinetic energy of the impacting particle and E_{th} is the threshold energy for sputtering related to mass ratios of M_1 and M_2 (Bohdansky, 1984). E_{th} must be greater than E_0 for sputtering to occur (Bohdansky, 1984; Behrisch & Eckstein, 2007). The function $s_n(\gamma)$ describes the screened Coulomb interactions (Matsunami et al., 1981),

$$s_n(\gamma) = \frac{3.411\sqrt{\gamma} ln(\gamma + 2.718)}{1 + 6.35\sqrt{\gamma} + \gamma(-1.708 + 6.882)\sqrt{\gamma}}, \quad (2)$$

where γ is defined as,

$$\gamma = \frac{M_2}{M_1 + M_2} \frac{a}{Z_1 Z_2 e^2} E_0. \quad (3)$$

The functional form for α is

$$\alpha = \begin{cases} 0.2 & M_2/M_1 \leq 0.5 \\ 0.3(M_2/M_1)^{2/3} & 0.5 < M_2/M_1 < 10 \end{cases} \quad (4)$$

Finally, R_p/R is a correction factor that mitigates the overestimation of deposited energy on the surface layer induced by α for light atmospheric particles, and is the ratio of the mean projected range to the mean penetrated path length (Bohdansky, 1984).

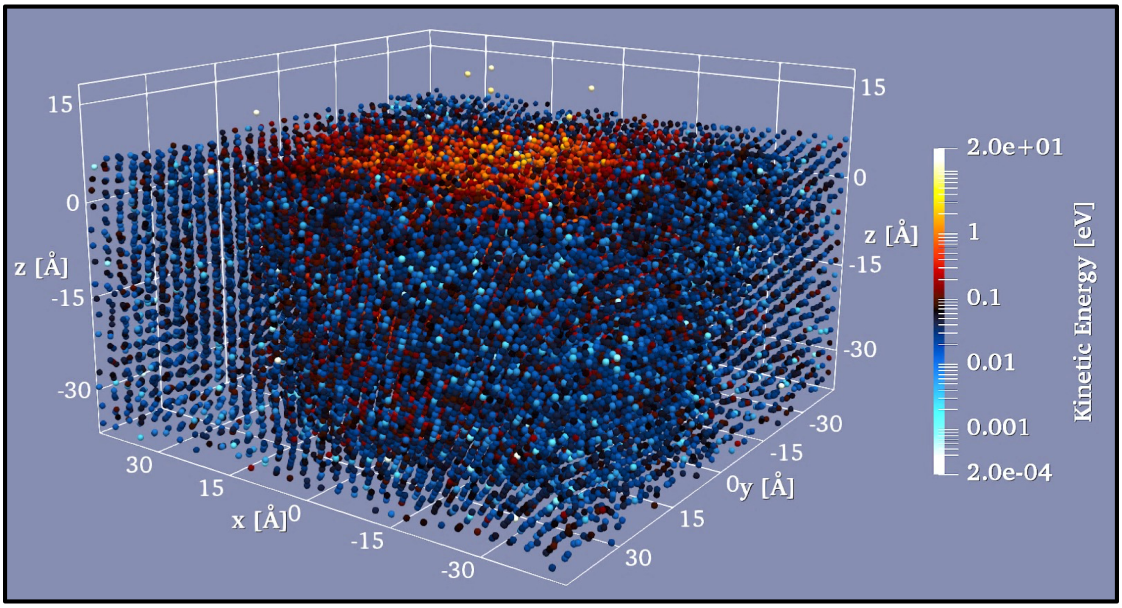

Figure 2. Snapshot of a simulation shortly after impact of a argon atom striking an iron meteoroid surface at 72 km/s. The impact site in this case is at $(x, y) = (0, 0)$ and the incident molecule is normal to the surface. Only a small part of the domain is shown; the boundaries are farther away than shown in this snapshot. The impacting molecule sputtered a handful of atoms from the meteoroid and increased the kinetic energy of the meteoroid atoms in the vicinity of the impact site.

Fig. 3 shows the sputtering yields for the atmospheric particles impacting iron in the first row and quartz in the second, calculated over 256 simulations. The red lines in the figure denote one and two standard deviations above the mean, representing the natural spread in the number of sputtered atoms over different simulation runs. Note that since the process is stochastic, the variance in the number of particles ejected per incident particle will not change much if even more impacts are simulated. The sputtering yield predicted by Eq. 1 is in blue for iron and purple for quartz. The sputtering yield from Eq. 1 is at most a factor of two off from the average sputtering yield found in the simulations. In all cases the model falls within a standard deviation of the average simulation result.

While Bohdansky, Lindner, Hechtl, Martinelli, and Roth (1986) found sputtering yield to be independent of temperature in a lab, Behrisch and Eckstein (1993) found a 30% increase in yield near sublimation temperatures for silver. Meteoroids heat as they descend into the atmosphere, so the sputtering and energy transfer from incident atmospheric particles with higher temperature targets warrants further investigation. Preliminary simulations with meteoroid targets at higher temperature, which will be reported in future work, suggest that the yield and energy transfer remain approximately the same for hotter targets, though this could change if the target has a surface in another phase.

2.3 Angular Dependence of Sputtering Yield

The simulations in Sec. 2.2 study impacts normal incidence, but particles will impact a meteoroid at a range of angles depending on the shape of the meteoroid. In this section, we examine the angular dependence. Sputtering yield models often define the yield at normal incidence (e.g. Eq. 1) and describe the angular dependence as a func-

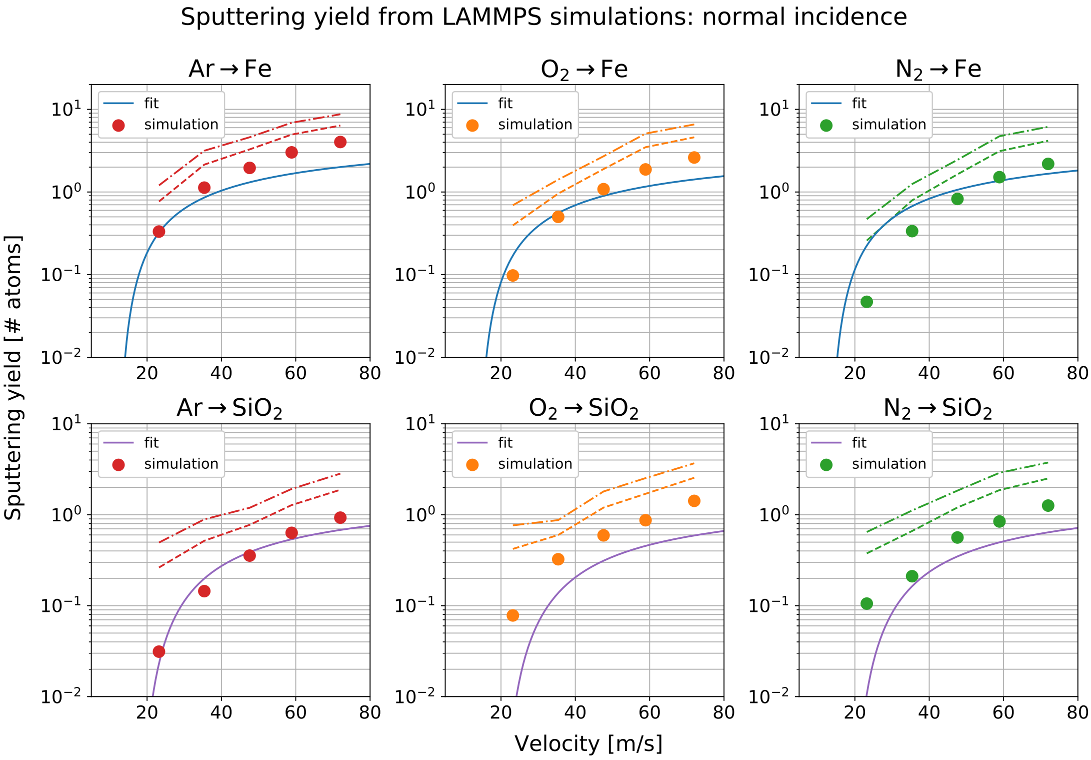

Figure 3. Sputtering yield at normal incidence for Ar (red), O_2 (orange), and N_2 (green) impacts on iron in the first row and quartz in the second, with 2 lines denoting one and two standard deviations above the mean. The blue (iron) or purple (quartz) line is the model (Eq. 1).

tion of the yield at normal incidence. Draine and Salpeter (1979) argue that $\langle Y(E_0, \theta)\rangle \approx 2Y(E_0, \theta = 0)$. Common approximations for the angular dependence are $Y(E_0, \theta_0)/Y(E_0, 0) = \cos^{-1}\theta$ at lower energies (Almén & Bruce, 1961; Molchanov & Telkovski, 1961; Sigmund, 1969; Draine & Salpeter, 1979; Rogers et al., 2005; Vondrak et al., 2008) and $Y(E_0, \theta_0)/Y(E_0, 0) = \cos^{-1.6}\theta$ at higher energies (Jurac et al., 1998). These forms have a clear problem in that they diverge for large angles ($\theta \to \pi/2$).

Eckstein and Preuss (2003) provide an empirical fit for sputtering yield as a function of angle:

$$\frac{Y(E_0, \theta_0)}{Y(E_0, 0)} = \left\{ \cos\left[\left(\frac{\pi}{2}\frac{\theta_0}{\theta_0^*}\right)^c\right]\right\}^{-f} \exp\left(b\left\{1 - 1\Big/\cos\left[\left(\frac{\pi}{2}\frac{\theta_0}{\theta_0^*}\right)^c\right]\right\}\right), \tag{5}$$

where b, c, and f are parameters to fit to experimental data. The variable θ_0^*, which is given by

$$\theta_0^* = \pi - \arccos\left(\sqrt{\frac{1}{1 + \frac{E_0}{E_{sp}}}}\right) \geq \frac{\pi}{2}, \tag{6}$$

is a parameter to negate the fact that a particle experiences a binding energy, E_{sp}, to the target, and cannot impact at an angle of 90° due to that non-zero energy of interaction between the projectile and target. For the cases presented here with argon, nitrogen, and oxygen, $E_{sp} \approx 0$ and $\theta_0^* \approx \pi$.

To examine the angular dependence of the sputtering yield, we use all of the same impactors (argon, nitrogen, and oxygen) and same meteoroid targets (iron and quartz) as the Section 2.2 at a meteoroid velocity of 59.8 km/s. Impact angles vary from 0° to 80° in 10° degree increments. For impacts at large angles, the simulations take considerably longer to resolve (up to 36 ps) compared to impacts at normal incidence (4 ps). Fig. 4 shows the angular dependence relative to the sputtering yield at normal incidence. We fit the simulation results to Eq. 5 for each case and list the parameters b, c, and f in legend of the Figure.

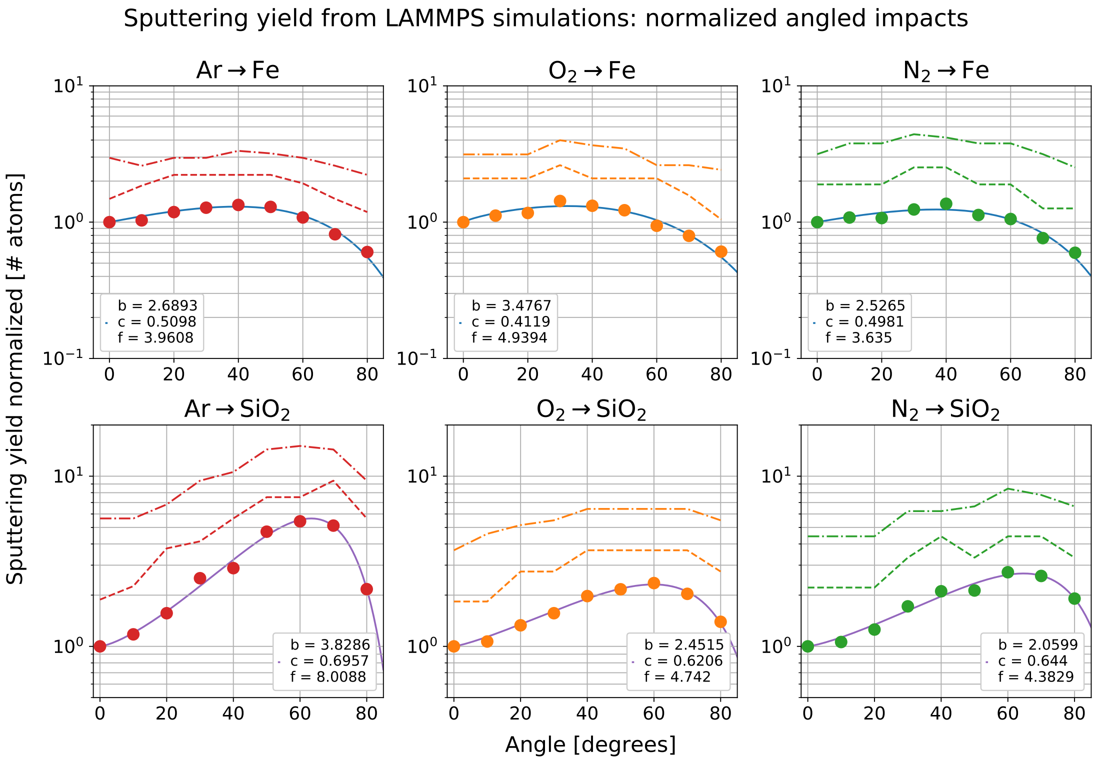

Figure 4. Sputtering yield versus angle for Ar, O_2, and N_2 impacts on iron in the top row and quartz on the bottom, normalized to $Y(E_0, 0)$. The two lines denote one and two standard deviations above the mean. The blue (iron) or purple (quartz) line is the Eq. 5, with the parameters in the legend

2.4 Sputtered Energy

MD simulations track the sputtered particle energies. The kinetic energy the particle in the last time-step within the bounds of the simulation defines the sputtered particle energy. At the point where a sputtered or reflected particle crosses the boundary, there is no interaction with the meteoroid atoms and its kinetic energy is constant. Recording the sputtered particle energies for each impact velocity and composition combination provides data for energy distribution histograms.

Figure 5 shows the distribution of the sputtered particle energy from Ar, O_2, and N_2 impacts on iron and quartz. More sputtering events occur at higher initial energies, given by Eq. 1, and therefore more overall entries in the histogram. The lower energy impacts have orders of magnitude smaller sputtering yields resulting in less total data from the same number of trials. The inverse gamma distribution is characterized by a steep initial rise, skewed shape, and the long tail that closely fit the histograms in Fig. 5. The parameters of the distribution (found in the legends in Fig. 5) are the shape param-

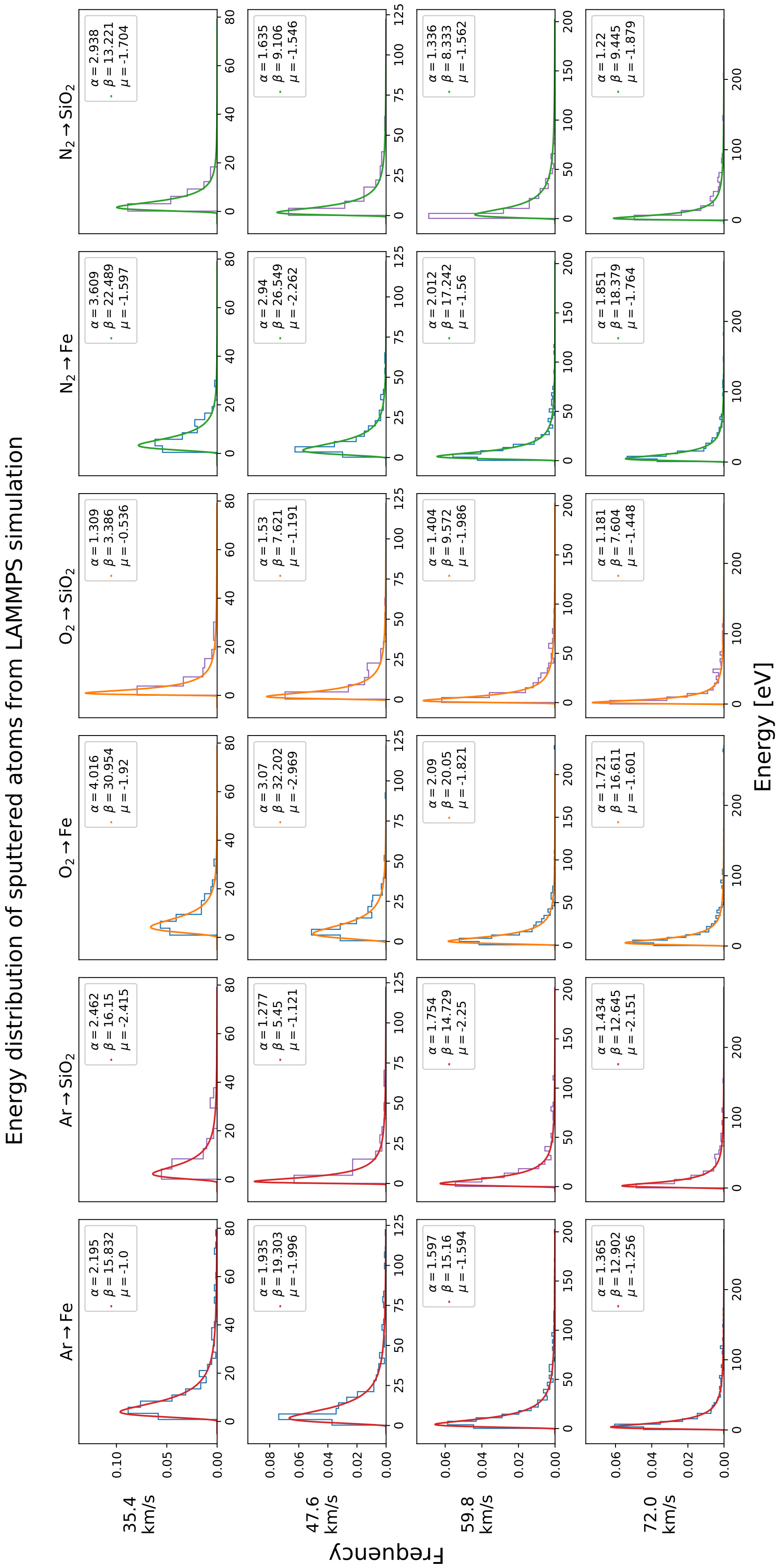

Figure 5. Histograms of energies of the sputtered particles from Ar, O_2 and N_2 impact. The parameters in the legends are the shape, scale, and location fit parameters.

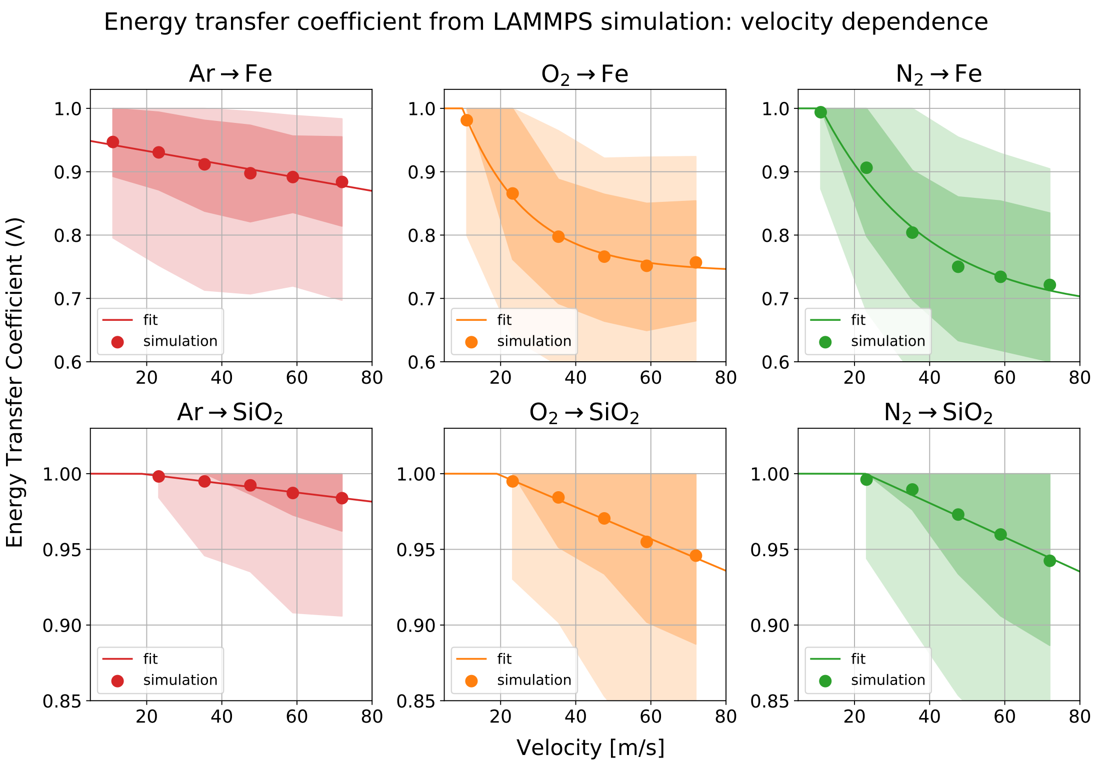

Figure 6. Energy as a function of angle for Ar, O_2, and N_2 impacts on iron and quartz, with fit for each atmospheric particle. The darker inner section is one standard deviation, and the lighter outer region is two standard deviations.

eter α, the scale parameter β, and location parameter μ. This probability distribution function was chosen over other PDFs like the Maxwell-Boltzmann distribution or the Gamma distribution simply due to its smaller residual value when fitting the simulation data.

2.5 Energy Transfer

The energy transfer is the fraction of the initial energy of the atmospheric particle transferred into the meteoroid surface. In this section, this coefficient refers to a single impact. Taking E_i, the initial energy of the atmospheric particle, and subtracting ΣE_s, the energies of any ricocheted atmospheric and sputtered particles from the LAMMPS simulations, gives the energy transferred to the meteoroid atoms. The increased energy kinetic energy of the meteoroids is equivalent to increased temperature of the meteoroid. The energy transfer coefficient is

$$\Lambda = \frac{E_i - \Sigma E_s}{E_i} \tag{7}$$

and characterizes the efficiency of energy transfer (and thus heating) based on a single impact. The energy transfer coefficient depends on velocity, angle, and projectile species. The simulation provides ΣE_s based on an input E_i, and the details of the atomic interactions, including energy lost to breaking bonds, are included in the MD simulation.

Fig. 6 shows the energy transfer coefficient for normal impacts of Ar, N_2 and O_2 on iron and quartz as a function of velocity. The sputtered atoms tend to play the smallest role in energy loss because ricocheting atmospheric atoms carry away most of the lost energy. The impacts on iron meteoroids have larger Λ on average because the iron lat-

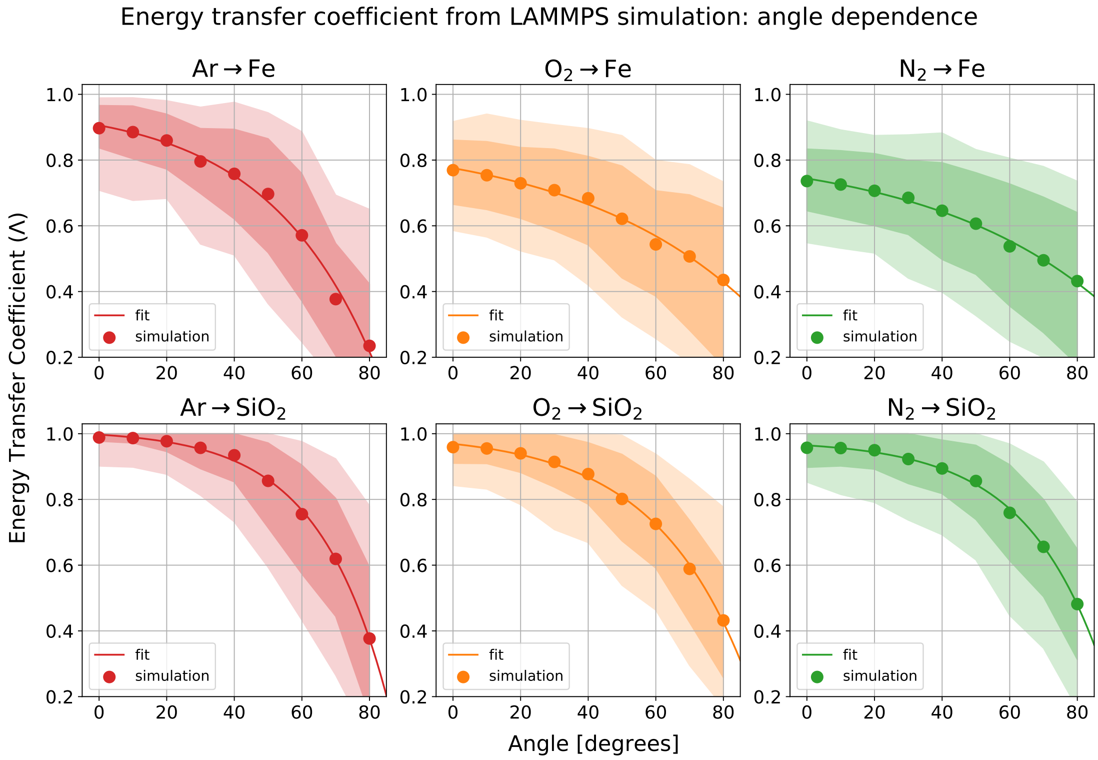

Figure 7. Energy transfer coefficient as a function of angle for Ar, O_2, and N_2 impacts on iron and quartz. The darker inner section is one standard deviation, and the lighter outer region is two standard deviations.

tice is more compact and tends to reflect the incident atmospheric particle more often. The energy transfer coefficient is closer to 1 for quartz due the crystal structure. The atmospheric particles embed themselves in the quartz surface more often due to the large gaps in the crystalline structure. O_2 and N_2 are similar in weight and chemical composition, and the bond dissociation energy is 5.165 eV for O_2 and 9.799 eV for N_2 (Darwent, 1970) (there is no bond energy for Ar, which is monatomic). The energy of the ricocheting nitrogen and oxygen atoms increases with initial energy, but at a slower rate than the decreasing fraction the bond dissociation energy in the total initial energy. Therefore the energy transfer coefficient of O_2 and N_2 decreases sharply at with increasing energy at the lowest energies, and (with lessening relevance of the bond energy) levels off at higher energies.

Fig. 7 shows the energy transfer coefficient as a function of impact angle. The energy transfer coefficient decreases with increasing angle. As the impacting particle's transverse energy increases (i.e. angle increases), it often bounces off the surface, imparting little energy as it ricochets. Applying these simulation results to determine Λ requires averaging over the angle and assuming a meteoroid shape. This is addressed in Section 3.2 below.

3 Ablation Model with a Modified Energy Transfer Coefficient

The LAMMPS simulations from the previous section provide the energy transfer coefficient as a function of velocity, material and angle. Applying the energy transfer coefficient results, we model the evolution of a meteoroid as it descends into the atmosphere using numerical meteoroid ablation model. Ablation models predict visual magnitude and electron line density, corresponding to optical and radar measurements respectively, from the ablation model output. Integrating over the surface of the meteoroid results in the energy transfer coefficient as a function of velocity and altitude.

3.1 Ablation Model

Sublimation is the final and the largest driver of meteoroid mass loss. Once the meteoroid has reached sublimation (sometimes referred to as thermal ablation) temperatures, the meteoroid begins to sublimate. Most meteoroids sublimate entirely into the atmosphere before striking the ground. The four coupled ordinary differential equations described below model this process. These equations follow work from Campbell-Brown and Koschny (2004), Rogers et al. (2005), and Vondrak et al. (2008).

The mass loss as a function of time resulting from sputtering (the first term) and sublimation (the second term),

$$\frac{dm}{dt} = -\left(\frac{3m\pi^{1/2}}{4\rho_m}\right)^{2/3} M_2 v \Sigma_i n_i Y(E_0,\theta)_i - \left(\frac{3m\pi^{1/2}}{4\rho_m}\right)^{2/3} \psi p_s \sqrt{\frac{\mu}{2\pi k_b T}} \tag{8}$$

where, m is the meteoroid mass, ρ_m is the meteoroid mass density, v is the velocity, and n_i and Y_i are the atmospheric number density and the sputtering yield of the i-th atmospheric species respectively. M_2 in the sputtering mass loss term is the meteoroid's average atomic mass, whereas μ is the meteoroid's average molecular mass, as sputtering dislodges single atoms and sublimation ejects entire molecules. The sublimation term uses the Clausius- Clapeyron equation for saturated vapor pressure, p_s, defined as

$$p_s = \exp\left(C - \frac{L\mu}{k_b T}\right) \tag{9}$$

where L is the latent heat of evaporation and C is a material dependent constant. ψ is the condensation probability coefficient, k_b is the Boltzmann constant, and T is the meteoroid temperature. The sublimation mass loss term primarily depends on the temperature of the meteoroid. Once the meteoroid has reached evaporation temperatures, p_s mainly governs how much mass is ejected during this stage of ablation.

The change in temperature of the meteoroid comes from conservation of energy, given by

$$\frac{1}{2}\Lambda\rho_{air}v^3 = 4\epsilon\sigma(T^4 - T_{air}^4) + \frac{c(m\rho_m^2)^{1/3}}{A}\frac{dT}{dt} - \frac{L}{A}\left(\frac{m}{\rho_m}\right)^{2/3}\frac{dm}{dt}_{sub} \tag{10}$$

The left hand side is the energy from the atmospheric particles. The energy transfer coefficient, Λ, is discussed in Section 2.5. The right hand side represents the energy lost to thermal radiation, meteoroid heating, and sublimation, respectively. In the radiation term, ϵ is the emissivity of the meteoroid, σ is Stefan-Boltzmann's constant, and T_{air} is the atmospheric temperature. In the heating term, c is the specific heat of the meteoroid, and dT/dt is the meteoroid temperature change as a function of time. In the sublimation term, $\frac{dm}{dt}_{sub}$ is the mass loss due to sublimation (the second term in Eq. 8).

The deceleration of the meteoroid,

$$\frac{dv}{dt} = -\frac{\Gamma A}{(m\rho_m^2)^{1/3}}\rho_{air}v^2 \tag{11}$$

comes from conservation of linear momentum of an object moving through a fluid. Γ is the drag coefficient, describing the efficiency of momentum transfer from atmospheric particle impacts. The the change in altitude as a function of time is given by

$$\frac{dh}{dt} = -v\cos(\chi) \tag{12}$$

where χ is the angle of entry into the atmosphere.

The intensity of the radiation the meteoroid produces as it ablates is given by

$$I = -\frac{1}{2}\tau_1 v^2 \frac{dm}{dt}. \tag{13}$$

The luminous efficiency factor, τ_1, is defined as

$$\tau_1 = 2\frac{\epsilon}{\mu}\frac{\zeta}{v^2} \tag{14}$$

where ϵ is the mean excitation energy, and μ is the molecular mass, and ζ, the excitation coefficient, is the sum of the excitation probabilities from atomic collisions (Jones & Halliday, 2001; Hill et al., 2005). The relationship between apparent visual magnitude and intensity is given by (Campbell-Brown & Koschny, 2004)

$$m_v = 6.8 - 1.086\ln I \tag{15}$$

Meteor radars detect the electron line density along the meteor path. The electron line density is defined in Jones (1997) as

$$q = \frac{\beta}{\mu v}\frac{dm}{dt}. \tag{16}$$

In Eq. 16, μ is the average ablated particle mass and dm/dt is the mass loss from Eq. 8. The β term is the ionization coefficient of an atom or molecule, and is a function of velocity, given by

$$\beta(v) = \beta_0(v) + 2\int_{v_0}^{v}\beta_0(v')dv' \tag{17}$$

where β_0 is the ionization probability of a meteoroid particle initial collision with an atmospheric particle (Jones, 1997).

Electron line density inferred from and visual magnitude are physical observables. Therefore solving Equations 8, 11, 10, 12, 15 and 16 simultaneously approximately models the evolution of a meteoroid traveling through an atmosphere. The modeled the visual magnitude can be compared to light curves of actual meteoroids and electron line density can be compared to radar measurements.

3.2 Microscopic Impacts to Macroscopic Meteoroid interactions

MD simulations in Section 2.5 provided the energy transfer coefficients (Λ) for single impacts at various velocities and angles. Integrating Λ from the simulations across a spherical meteoroid surface, taking into account impacts from all angles 0-90°, yields the energy transfer coefficient, $\langle\Lambda(v)\rangle_\theta$, in Eq. 10 for each particle species, impacting either an iron or quartz meteoroid. Fig. 8 shows Λ values of impacts on a spherical meteoroid, for the atmospheric species N_2, O_2, and Ar, calculated in this manner. The black line in Fig. 8 is the energy transfer coefficient as a function of velocity using atmospheric density ratios at 100km altitude.

The assumption that the angle averaged sputtering yield, $\langle Y(E)\rangle_\theta$, is twice the normal yield, is often used while solving for the sputtering portion of the mass loss term in numerical models (Draine, 1977; Draine & Salpeter, 1979; Rogers et al., 2005; Vondrak et al., 2008; Briani et al., 2013). The MD simulations suggest this can be inaccurate, especially for iron. We found that the angle averaged sputtering yield for Argon, O_2, and

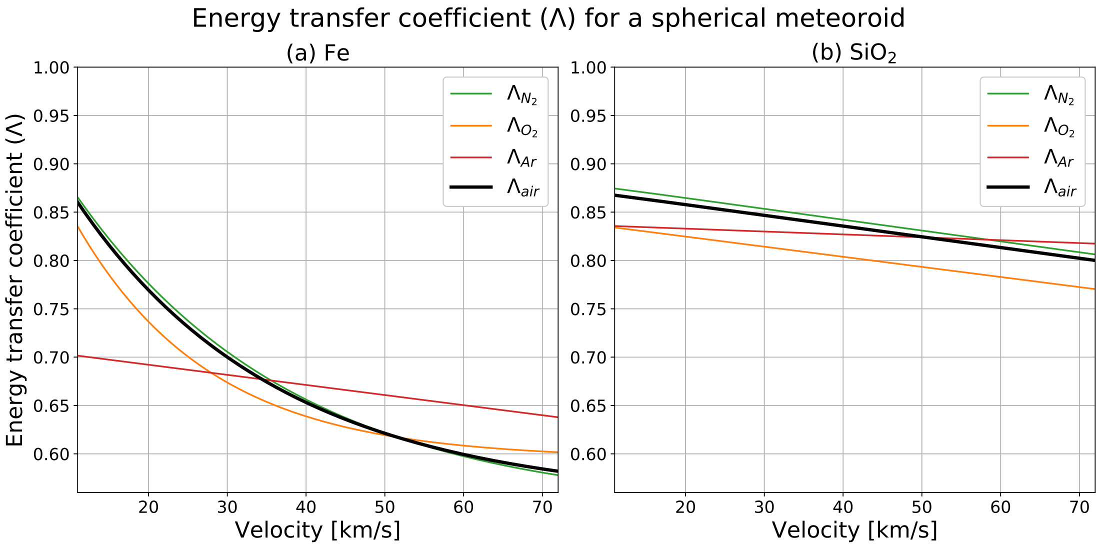

Figure 8. The energy transfer coefficient, Λ, as a function of velocity for both iron and quartz determined from MD simulations in Section . The three atmospheric species are in red, green, and orange, with the black line denoting the thermal energy transfer coefficient of air at 100 km altitude.

N_2 impacting iron is 1.137, 1.124 and 1.088 times the sputtering yield of normal impacts respectively. For quartz, we found the angle averaged yield for the same particles is 3.466, 1.840, and 2.018, respectively.

Our model uses atmospheric parameters from MSISE20000, (Picone et al., 2002), and Λ used in Eq. 10 depends on atmospheric composition. Fig. 9a displays the number density from NRLMSISE-00 from 0 to 300 km. Fig. 9b shows the Knudsen number as a function of altitude for a range of meteoroids. The Knudsen number is $\text{Kn} = \lambda/L$, where λ is the mean free path of the atmosphere and L is the characteristic length of the meteoroid. For typical ablation altitudes and small meteoroids $\text{Kn} \gg 1$, which means the meteoroid experiences individual impacts of atmospheric particles instead of fluid drag (Sharipov, 2007). This justifies treating the impacts as separate and summing their effects.

Eqs. 8-12 were solved using a variable-coefficient solver with a fixed-coefficient backward differentiation formula applicable to stiff problems. We solved the equations twice for each initial condition, once with $\Lambda = 1$, and once Λ calculated as a function of velocity and atmospheric composition. Initial masses ranged from 1×10^{-12} kg to 9×10^{-6} kg and velocities ranged from 11 km/s to 72 km/s. The models used the same velocities as in the MD simulations, and 5 different masses per order of magnitude.

Fig. 10 shows the results from the ablation model for an iron meteoroid with and initial mass of 1 μg and velocity of 59.8 km/s. The dotted line sets $\Lambda = 1$ and the solid line uses the calculated $\Lambda < 1$. The meteoroid heats at a slower rate with $\Lambda < 1$ as expected. Λ is 15-40% lower for iron and 10-25% lower for stony meteoroids. The slower heating rate affects the rate of mass loss, the visual intensity (Eq. 15), in purple, and the electron line density (Eq. 16), in green. In Fig. 10 the altitude of the maximum visual magnitude and electron line density differs by 2.5km with different Λ.

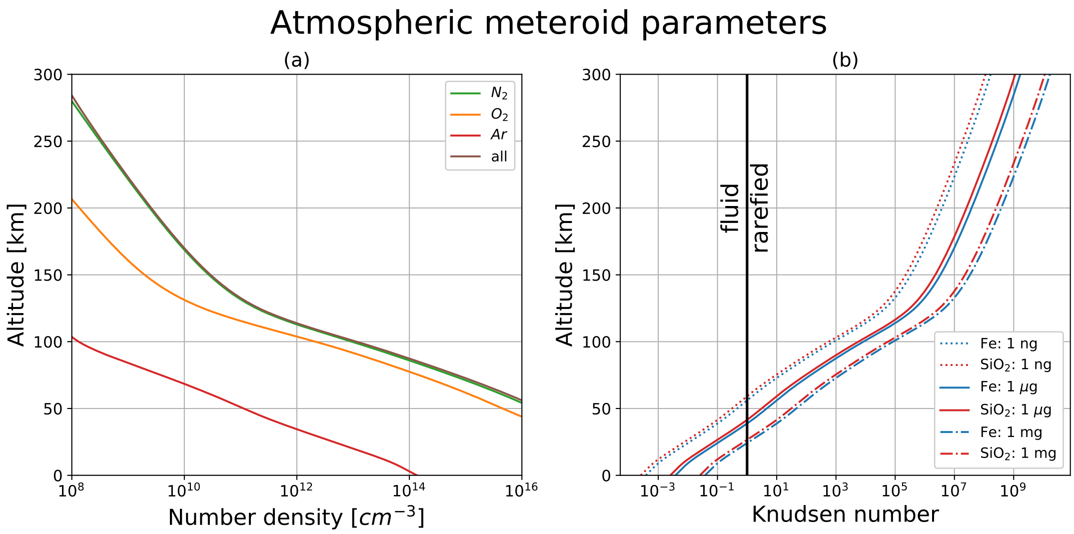

344 **Figure 9.** Atmospheric parameters with species and total number density from 0 to 300 km in
345 altitude (a) and Knudsen number for different meteoroids (b).

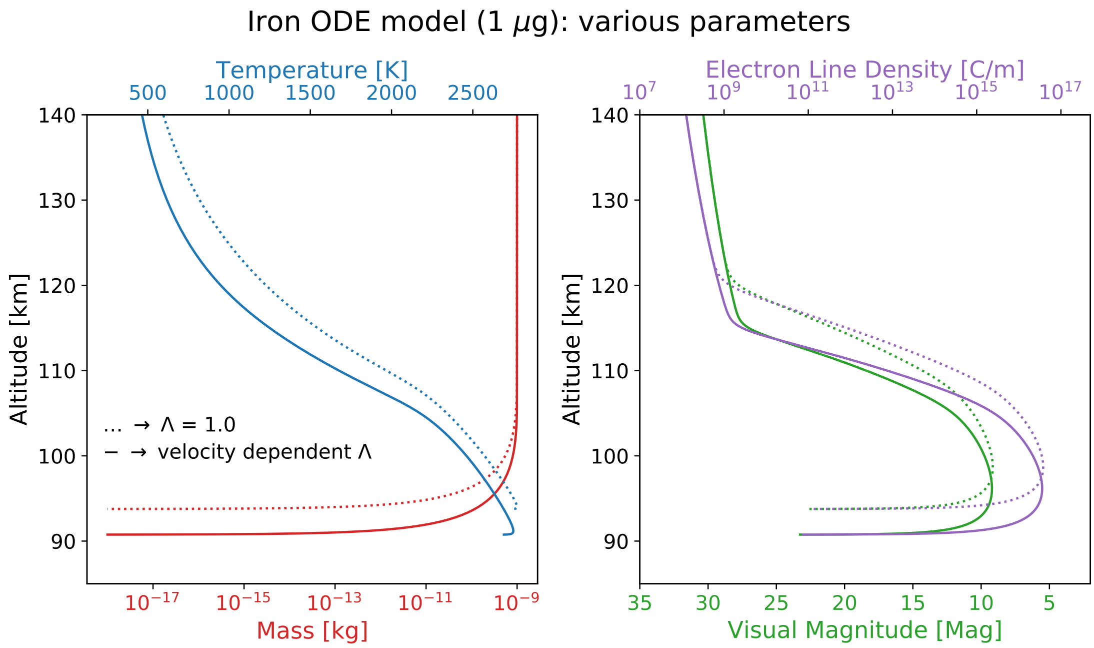

359 **Figure 10.** Results from the ablation model for an iron meteoroid with an initial mass of 1
360 μg and initial velocity of 59.8 km/s. The left plot shows meteoroid temperature and mass, with
361 the dotted line indicating the model with Λ=1.0 and the solid line indicating the model with
362 $\Lambda < 1$. The right plot shows visual magnitude and electron line density as calculated by Eq. 15
363 and Eq. 16 respectively.

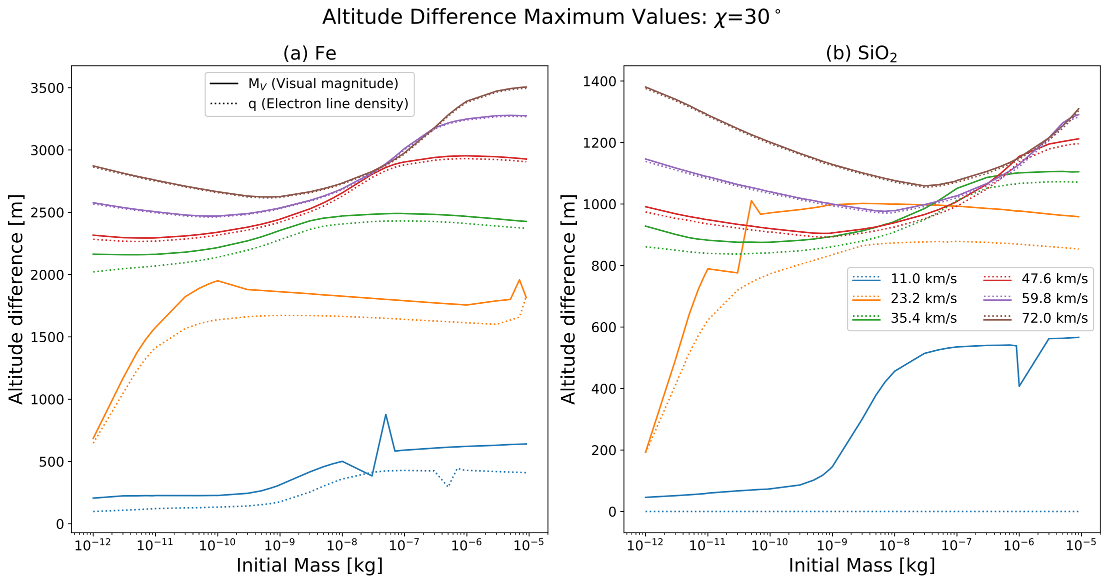

Figure 11. Relationship between altitude difference of the maximum value of visual magnitude and electron line density, and the initial masses, of the numerical model where $\Lambda = 1$ and $\Lambda < 1$. The solid line and the dotted line is the altitude difference for visual magnitude (M_V) and the electron line density (q) respectively. The figure on the left show the results for an iron meteoroid and on the right show the results for a quartz meteoroid.

3.3 Observable Parameters

We compare the effect of the simulation-derived energy transfer coefficient to the assumption that $\Lambda = 1$ by contrasting the altitude of maximum values of the visual magnitude and electron line density from the ablation model. The meteoroid masses range from the largest meteoroid in the valid free-molecular flow regime (10^{-6} kg) to the smallest meteoroids detectable by radar (10^{-12} kg). Fig. 11 shows the difference in altitude of the maximum visual magnitude and electron line density between the $\Lambda = 1$ and the $\Lambda < 1$ solutions.

In Fig. 11 show the altitude difference of the electron line density and visual magnitude respectively for iron quartz meteoroids. The infrequent departures from smoothness are a result of imperfect interpolation of atmospheric parameters to the meteoroid location at any given time. The change in altitude for quartz is less than for iron because the energy transfer coefficient for quarts is closer to one, because it loses less energy to ricochet and sputtered particles, as shown in Sec. 2.5.

Quartz's threshold velocity for ionization is around 12.9 km/s, so the electron line density from the 11.0 km/s run is zero across all masses. Otherwise in Fig. 11b the altitude difference is fairly constant across the masses, and tends towards a difference of 1000-1300 meters. Lower initial velocities (11.0 and 23.2 km/s) have smaller altitude differences due to the meteoroids decelerating to below the threshold velocities for visual magnitude, (6.8 km/s, per the relation for η in Eq. 14). The altitude difference in electron line density and visual magnitude begins to diminish at the threshold velocity more quickly at 23.2 for masses over 1μg due to the $m^{-1/3}$ factor in Eq. 11.

Iron's three fastest velocities' altitude differences group together between 2500 and 3500 meters. This occurs because of the small range of the energy transfer coefficient at higher velocities for N_2 and O_2 in Fig. 6 results in similar heating rates. The smallest initial masses, especially at high velocities, sublimate very quickly. This results in the high velocity altitude differences decreasing from 10^{-12} kg to 10^{-9}kg. The increase in the altitude differences for heavier meteoroids comes from the duration sputtering period. The maximum rate of mass loss occurs right at the beginning of sublimation. The heating rate (determined by the energy transfer coefficient) determines the duration of sputtering period and the altitude where the meteoroid begins sublimation. The sputtering period increases with mass as the heavier meteoroids require more impacts to reach sublimation temperatures than smaller meteoroids or their $\Lambda = 1$ counterparts.

4 Conclusions

Molecular dynamics simulation of atomic scale sputtering on the surface of meteoroids due to atmospheric particle impacts show how energy transfer from the atmosphere depends on the species, velocity, angle, and meteoroid material. Single particle impacts are important not only for sputtering, but for sublimation as well, since the dynamics of the single impacts govern how quickly a meteoroid gains thermal energy. Applying a more accurate energy transfer coefficient adds an additional level of accuracy to models of meteoroid ablation in the atmosphere. Here we present our main conclusions, both from the MD simulations and the numerical ablation models:

1. Sputtering yield at normal incidence found by the LAMMPS simulations follows the incident energy dependent equation put forth by Tielens et al. (1994) within a factor of 2 for iron and an order of magnitude for quartz.
2. Sputtering yield at various angles was found to best fit the empirical normalized yield equation from Eckstein and Preuss (2003), which differs greatly from generally assumed distributions (e.g. Jurac et al. (1998), Rogers et al. (2005)).
3. The MD data shows that the impacting energy is not entirely incorporated into the meteoroid as assumed in many ablation models. Instead, the energy transfer coefficient depends on incident velocity and meteoroid material.
4. Applying the newly derived energy transfer coefficient to the ablation model predict that observable parameters reach their peak at lower altitudes (3.5 km difference for iron and 1.3 km difference for quartz).

Currently, we lack a complete profile of meteoroid energy transfer coefficients, as we did not examine the temperature dependence. Future work will involve using MD simulations to model meteoroids with elevated temperatures and the sublimation process. This will allow us to determine temperature dependent sputtering rates and energy transfer coefficient.

Acknowledgments

This work is supported by NSF Grant AGS-1755020, NSF Grant AGS-1755350, NSF-AGS Postdoctoral Research Fellowship Award No. 143353, Naval Research Laboratory Base Program, and the Boston University Undergraduate Research Opportunities Program. This work used the Extreme Science and Engineering Discovery Environment (XSEDE), which is supported by National Science Foundation grant ACI-1548562. The authors acknowledge the Texas Advanced Computing Center (TACC) at The University of Texas at Austin for providing HPC resources that have contributed to the research results reported within this paper; URL: http://www.tacc.utexas.edu. Data is availible online (https://doi.org/10.7910/DV

References

Almén, O., & Bruce, G. (1961). Collection and sputtering experiments with noble gas ions. *Nucl. Instrum. Methods*, *11*, 257–278. Retrieved from http://www.sciencedirect.com/science/article/pii/0029554X6190026X doi: https://doi.org/10.1016/0029-554X(61)90026-X

Behrisch, R., & Eckstein, W. (1993). Sputtering yield increase with target temperature for ag. *Nucl. Instrum. Methods Phys. Res. B*, *82*(2), 255–258. doi: https://doi.org/10.1016/0168-583X(93)96027-A

Behrisch, R., & Eckstein, W. (2007). *Sputtering by particle bombardment: Experiments and computer calculations from threshold to mev energies* (Vol. 110). Berlin: Springer.

Berthelot, D. (1898). Sur le mélange des gaz. *C. R. Hebd. Seances Acad. Sci*, *126*(1), 1703–1855. Retrieved from http://visualiseur.bnf.fr/CadresFenetre?O=NUMM-3082&I=1703&M=notice doi: 10.1002/andp.18812480110

Bohdansky, J. (1984). A universal relation for the sputtering yield of monatomic solids at normal ion incidence. *Nucl. Instrum. Methods Phys. Res. B*, *2*(1), 587–591.

Bohdansky, J., Lindner, H., Hechtl, E., Martinelli, A., & Roth, J. (1986). Sputtering yield of cu and ag at target temperatures close to the melting point. *Nucl. Instrum. Methods Phys. Res. B*, *18*(1), 509–514. doi: https://doi.org/10.1016/S0168-583X(86)80078-7

Bouneau, S., Brunelle, A., Della-Negra, S., Depauw, J., Jacquet, D., Le Beyec, Y., ... Andersen, H. (2002, 03). Very large gold and silver sputtering yields induced by kev to mev energy au_*n* clusters (n = 1-13). *Phys. Rev. B*, *65*(14), 144106-1–144106-8. doi: 10.1103/PhysRevB.65.144106

Briani, G., Pace, E., N. Shore, S., Pupillo, G., Passaro, A., & Aiello, S. (2013, 02). Simulations of micrometeoroid interactions with the earth atmosphere. *Astron. Astrophys.*, *552*, A53. doi: 10.1051/0004-6361/201219658

Campbell-Brown, M., & Koschny, D. (2004, 05). Model of the ablation of faint meteors. *Astron. Astrophys.*, *418*, 751-758. doi: 10.1051/0004-6361:20041001-1

Ceplecha, Z., Borovička, J., Elford, W. G., ReVelle, D. O., Hawkes, R. L., Porubčan, V., & Šimek, M. (1998). Meteor phenomena and bodies. *Space Sci. Rev*, *84*(3), 327–471. Retrieved from https://doi.org/10.1023/A:1005069928850 doi: 10.1023/A:1005069928850

Cheney, K. B., Rogers, E. E., & Pitkin, E. T. (1963, 07). *Research on experimental evaluation of sputtering yield rates* (Tech. Rep.). MARQUARDT CO VAN NUYS CA.

Darwent, B. (1970). *Bond dissociation energies in simple molecules* (No. 31). U.S. National Bureau of Standards. Retrieved from https://books.google.com/books?id=QoXMYOgi8CkC

DeLuca, M., & Sternovsky, Z. (2019). High-speed drag measurements of aluminum particles in free molecular flow. *Journal of Geophysical Research: Space Physics*, *124*(5), 3743–3751. Retrieved from https://agupubs.onlinelibrary.wiley.com/doi/abs/10.1029/2019JA026583 doi: 10.1029/2019JA026583

Dimant, Y. S., & Oppenheim, M. M. (2017a). Formation of plasma around a small meteoroid: 1. kinetic theory. *J. Geophys. Res. Space Physics*, *122*(4), 4669–4696. Retrieved from https://agupubs.onlinelibrary.wiley.com/doi/abs/10.1002/2017JA023960 doi: 10.1002/2017JA023960

Dimant, Y. S., & Oppenheim, M. M. (2017b). Formation of plasma around a small meteoroid: 2. implications for radar head echo. *J. Geophys. Res. Space Phys.*, *122*(4), 4697-4711. Retrieved from https://agupubs.onlinelibrary.wiley.com/doi/abs/10.1002/2017JA023963 doi: 10.1002/2017JA023963

Draine, B. T. (1977). Center for radiophysics and space research report no. 669. Cornell University.

Draine, B. T., & Salpeter, E. E. (1979, 8). On the physics of dust grains in hot gas. *Astrophys. J.*, *231*, 77–94. doi: 10.1086/157165

Eckstein, W., & Preuss, R. (2003). New fit formulae for the sputtering yield. *J.*

Nucl. Mater., *320*(3), 209–213. Retrieved from http://www.sciencedirect.com/science/article/pii/S0022311503001922 doi: https://doi.org/10.1016/S0022-3115(03)00192-2

Elliott, R. S. (2018). *Efficient 'universal' shifted lennard-jones model for all kim api supported species developed by elliott and akerson (2015) v003.* OpenKIM. (Online; accessed: 2019-03-24) doi: 10.25950/962b4967

Hill, K. A., Rogers, L. A., & Hawkes, R. L. (2005, 12). High geocentric velocity meteor ablation. *Astron. Astrophys.*, *444*, 615–624. doi: 10.1051/0004-6361:20053053

Jones, W. (1997, 06). Theoretical and observational determinations of the ionization coefficient of meteors. *Mon. Notices Royal Astron. Soc.*, *288*(4), 995-1003. doi: 10.1093/mnras/288.4.995

Jones, W., & Halliday, I. (2001, 02). Effects of excitation and ionization in meteor trains. *Mon. Not. R. Astron. Soc.*, *320*(4), 417-423. Retrieved from https://doi.org/10.1046/j.1365-8711.2001.03833.x doi: 10.1046/j.1365-8711.2001.03833.x

Jurac, S., Johnson, R. E., & Donn, B. (1998, aug). Monte carlo calculations of the sputtering of grains: Enhanced sputtering of small grains. *Astrophys. J.*, *503*(1), 247–252. Retrieved from https://doi.org/10.10862F305994 doi: 10.1086/305994

Krebs, K. H. (1977). *Investigations on sputtering and secondary ion yield from metals under bombardment of noble gases in the energy range 5 - 25kev.* IAEA, Vienna.

Laegreid, N., & Wehner, G. K. (1961). Sputtering yields of metals for ar$^+$ and ne$^+$ ions with energies from 50 to 600 ev. *J. Appl. Phys.*, *32*(3), 365–369. Retrieved from https://doi.org/10.1063/1.1736012 doi: 10.1063/1.1736012

Lebedinets, V. N., & Shushkova, V. B. (1970, 11). Micrometeorite sputtering in the ionosphere. *Planet. Space Sci.*, *18*, 1653–1659. doi: 10.1016/0032-0633(70)90039-5

Lorentz, H. A. (1881). Ueber die anwendung des satzes vom virial in der kinetischen theorie der gase. *Ann. Phys. (Berl.)*, *248*(1), 127–136. Retrieved from https://onlinelibrary.wiley.com/doi/abs/10.1002/andp.18812480110 doi: 10.1002/andp.18812480110

Love, S. G., & Brownlee, D. E. (1991). Heating and thermal transformation of micrometeoroids entering the earth's atmosphere. *Icarus*, *89*(1), 26–43. Retrieved from http://www.sciencedirect.com/science/article/pii/0019103591900858 doi: https://doi.org/10.1016/0019-1035(91)90085-8

Matsunami, N., Yamamura, Y., Itikawa, Y., Itoh, N., Kazumata, Y., Miyagawa, S., … Shimizu, R. (1981). A semiempirical formula for the energy dependence of the sputtering yield. *Radiat. Eff.*, *57*(1–2), 15–21. doi: 10.1080/01422448008218676

Molchanov, V. A., & Telkovski, V. G. (1961). The variation of the cathode dissipation coefficient, as dependent on the angle at which the ions are striking the target. *Proc. USSR Acad. Sci.*, *136*, 801–802. Retrieved from http://mi.mathnet.ru/dan24584

Müller, M., Erhart, P., & Albe, K. (2007, jul). Analytic bond-order potential for bcc and fcc iron—comparison with established embedded-atom method potentials. *J. Phys. Condens. Matter*, *19*(32), 326220. Retrieved from https://doi.org/10.1088\%2F0953-8984\%2F19\%2F32\%2F326220 doi: 10.1088/0953-8984/19/32/326220

Munetoh, S., Motooka, T., Moriguchi, K., & Shintani, A. (2007, 4 1). Interatomic potential for si-o systems using tersoff parameterization. *Comput. Mater. Sci.*, *39*(2), 334–339. doi: 10.1016/j.commatsci.2006.06.010

Picone, J. M., Hedin, A. E., Drob, D. P., & Aikin, A. C. (2002). Nrlmsise-00 empirical model of the atmosphere: Statistical comparisons and scientific issues.

J. Geophys. Res. Space Phys., *107*(A12), SIA 15-1-SIA 15-16. Retrieved from https://agupubs.onlinelibrary.wiley.com/doi/abs/10.1029/2002JA009430 doi: 10.1029/2002JA009430

Plimpton, S. (1995). Fast parallel algorithms for short-range molecular dynamics. *J. Comput. Phys*, *117*(1), 1–19. Retrieved from http://www.sciencedirect.com/science/article/pii/S002199918571039X doi: https://doi.org/10.1006/jcph.1995.1039

Plimpton, S. J., & Thompson, A. P. (2012). Computational aspects of many-body potentials. *MRS Bulletin*, *37*(5), 513-521. doi: 10.1557/mrs.2012.96

Popova, O. P., Strelkov, A. S., & Sidneva, S. N. (2007). Sputtering of fast meteoroids' surface. *Advances in Space Research*, *39*(4), 567–573. doi: 10.1016/j.asr.2006.05.008

Rogers, L. A., Hill, K. A., & Hawkes, R. L. (2005). Mass loss due to sputtering and thermal processes in meteoroid ablation. *Planet. Space Sci.*, *53*(13), 1341 - 1354. Retrieved from http://www.sciencedirect.com/science/article/pii/S0032063305001479 doi: https://doi.org/10.1016/j.pss.2005.07.002

Sandia National Labs, & Temple University. (2013). *Overview of lammps.* Retrieved from https://lammps.sandia.gov/doc/Intro_overview.html

Sharipov, F. (2007, 01). Rarefied gas dynamics and its applications to vacuum technology. *CAS 2006 - CERN Accelerator School: Vacuum in Accelerators, Proceedings*, 1-13.

Sigmund, P. (1969, Aug). Theory of sputtering. i. sputtering yield of amorphous and polycrystalline targets. *Phys. Rev.*, *184*, 383–416. Retrieved from https://link.aps.org/doi/10.1103/PhysRev.184.383 doi: 10.1103/PhysRev.184.383

Szasz, C., Kero, J., Pellinen-Wannberg, A., Meisel, D. D., Wannberg, G., & Westman, A. (2008, 6 01). Estimated visual magnitudes of the eiscat uhf meteors. *Earth, Moon, and Planets*, *102*(1), 373–378.

Tersoff, J. (1988, 4). New empirical approach for the structure and energy of covalent systems. *Phys. Rev. B*, *37*, 6991–7000. Retrieved from https://link.aps.org/doi/10.1103/PhysRevB.37.6991 doi: 10.1103/PhysRevB.37.6991

Thomas, E. W. (2017). *Laboratory simulations of micrometeoroid ablation* (PhD Dissertation). University of Colorado at Boulder.

Tielens, A. G. G. M., McKee, C. F., & Seab, H. D. J., C. G. (1994). The physics of grain-grain collisions and gas-grain sputtering in interstellar shocks. *Astrophys. J.*, *431*(1), 321–340. doi: 10.1086/174488

Tsunoyama, K., Suzuki, T., & Ohashi, Y. (1976, 02). Sputtering of iron with ion beams of o2+, n2+ and ar+. *Japanese Journal of Applied Physics*, *15*(2), 349–355. doi: 10.1143/jjap.15.349

Urbassek, H. M. (1997). Molecular-dynamics simulation of sputtering. *Nuclear Instruments and Methods in Physics Research Section B: Beam Interactions with Materials and Atoms*, *122*(3), 427–441. Retrieved from http://www.sciencedirect.com/science/article/pii/S0168583X96006817 (Nanometric Phenomena Induced by Laser, Ion and Cluster Beams) doi: https://doi.org/10.1016/S0168-583X(96)00681-7

Varga, P., Neidhart, T., Sporn, M., Libiseller, G., Schmid, M., Aumayr, F., & Winter, H. P. (1997, 01). Sputter yields of insulators bombarded with hyperthermal multiply charged ions. *Physica Scripta*, *T73*, 307–310. doi: 10.1088/0031-8949/1997/t73/100

Vida, D., Brown, P. G., & Campbell-Brown, M. (2018, 07). Modelling the measurement accuracy of pre-atmosphere velocities of meteoroids. *Monthly Notices of the Royal Astronomical Society*, *479*(4), 4307-4319. Retrieved from https://doi.org/10.1093/mnras/sty1841 doi: 10.1093/mnras/sty1841

Vondrak, T., Plane, J. M. C., & Broadley, D., S.; Janches. (2008). A chemical model of meteoric ablation. *Atmospheric Chem. Phys*, *8*(23), 7015–7031. doi: 10

.5194/acp-8-7015-2008

Zhou, L. G., & Huang, H. (2013). Response embedded atom method of interatomic potentials. *Phys. Rev. B*, *87*(4), 045431. doi: 10.1103/PhysRevB.87.045431

Zoerb, K., Williams, J., Williams, D., & Yalin, A. (2005). *Differential sputtering yields of refractory metals by xenon, krypton, and argon ion bombardment at normal and oblique incidences.* The 29th International Electric Propulsion Conference, Princeton University, New Jersey.